



Failure mode transition speeds in an impact loaded prenotched plate with four thermoviscoplastic relations

R. C. BATRA and N. A. JABER

Department of Engineering Science and Mechanics, M/C 0219, Virginia Polytechnic Institute and State University, Blacksburg, VA 24061, USA

Received 31 May 2000; accepted in revised form 9 January 2001

Abstract. Four different thermoviscoplastic relations, namely, the Litonski–Batra, Johnson–Cook, Bodner–Partom and the power law are used to model the thermoviscoplastic response of a material. Each one of these relations accounts for strain hardening, strain-rate hardening and thermal softening of the material. The material parameters in these relations are found by solving an initial-boundary-value problem corresponding to simple shearing deformations so that the computed effective stress vs. the effective plastic strain curves match closely with the experimental data of Marchand and Duffy who tested thin-walled HY-100 steel tubes in torsion. These four viscoplastic relations are used to analyze dynamic thermomechanical deformations of a prenotched plate impacted on the notched side by a cylindrical projectile made of the same material as the plate. The impact loading on the contact surface is simulated by prescribing the time history of the normal component of velocity and null tangential tractions. A plane strain state of deformation is assumed to prevail in the plate and its deformations are studied for different values of the impact speed. The in-house developed finite element code employs constant strain triangular elements, one point integration rule, and a lumped mass matrix. The Lagrangian description of motion is used to describe deformations of the plate. The coupled nonlinear partial differential equations are first reduced to coupled nonlinear ordinary differential equations (ODEs) by using the Galerkin approximation. The ODEs are integrated by using the stiff solver, LSODE, which adaptively adjusts the time step size and computes the solution within the prescribed accuracy. Results computed with the four constitutive relations are found to be qualitatively similar to each other and the general trends agree with the experimental observations in the sense that at low speed of impact, a brittle failure ensues at a point on the upper surface of the notch tip. However, at high impact speeds, a ductile failure in the form of a shear band initiates first from a point on the lower surface of the notch tip. The predicted speed at which the failure mode transitions from brittle to ductile is different for the four viscoplastic relations. The effects of the notch tip radius and the yield strength of the material in a quasistatic simple tension/compression test on the failure-mode transition speed have been ascertained.

Key words: Finite element solution, microporous thermoviscoplastic material, transient plane strain deformations, brittle and ductile failures.

1. Introduction

During impact loading of pre-notched plates, Kalthoff (1987) and Kalthoff and Winkler (1987) observed that with an increase in the impact speed, the failure mode changed from brittle failure at a point on the upper surface of the notch tip to ductile failure in the form of a shear band initiating from a point on the lower surface of the notch tip; the lower surface of the notch is adjacent to the impacted edge of the plate. However, in the Charpy V-notch test, ductile failure ensues at low loading rates or at high temperatures and brittle failure at high loading rates or at low temperatures. Tvergaard and Needleman (1986, 1993) and Needleman and Tvergaard (1995) have numerically analyzed thermomechanical deformations of these two configurations by using Gurson's (1977) flow potential and a power law type

thermoviscoplastic relation. They showed that predictions from the same set of governing equations are in qualitative agreement with the seemingly contradictory observations in the two tests. Needleman and Tvergaard (1995), Zhou et al. (1996b), Batra and Nechitailo (1997), Batra and Gummalla (2000) and Batra and Ravisankar (2000) have numerically studied the Kalthoff problem. Whereas Needleman and Tvergaard and Zhou et al. employed a power law type relation to model the strain hardening and strain-rate hardening of the material, Batra et al. used the Johnson–Cook (1983) relation. None of these studies computed the impact speed at which the failure mode transition occurs. Also, it will be interesting to compare the thermomechanical response predicted by different thermoviscoplastic relations after they have been calibrated with the same set of test data. Batra and Kim (1990) conducted such studies for the initiation and development of an adiabatic shear band in a thermoviscoplastic body deformed in simple shear, and Batra and Jayachandran (1992) and Batra and Adam (1991) used different relations to analyze the steady state penetration of a thermoviscoplastic target by a rigid hemispherical nosed penetrator.

We use four thermoviscoplastic relations, namely, the Litonski–Batra, the Johnson–Cook, the Bodner–Partom and a power law to analyze the plane strain thermomechanical deformations of a prenotched plate used in Kalthoff’s experiments. We note that the only mechanical property listed in Kalthoff’s paper is the quasistatic yield strength of the material of the plate. We use values of material parameters, modified to the case of three-dimensional deformations, that Batra and Kim (1990) found by calibrating the four thermoviscoplastic relations against the experimental data of Marchand and Duffy (1988) who tested thin-walled HY100 steel tubes in torsion. Batra and Kim (1990) assumed that deformation of the material near the middle of the tube corresponded to that of simple shearing and determined the values of material parameters by solving an initial-boundary-value problem till the computed stress-strain curve at a nominal strain rate of 3300/s matched closely with that obtained from the test data. It is found that the four viscoplastic relations predict different values of the impact speed at which the failure mode in the Kalthoff problem changes from brittle to ductile. However, the qualitative nature of results computed with the four thermoviscoplastic relations is the same. We use the Bodner–Partom relation to ascertain the effect of the notch tip radius and the power law to scrutinize the effect of the quasistatic yield stress of the material on the transition speed.

2. Formulation of the problem

A schematic sketch of the problem studied is depicted in Figure 1. A cylindrical rod of diameter equal to the distance between the two notches in a prenotched plate strikes the side of the plate at normal incidence with speed v_0 . The cylindrical rod and the plate are made of the same microporous material and the plate before being impacted rests on a smooth rigid surface. We assume that a plane strain state of deformation prevails in the plate. The three-dimensional numerical solution of the problem by Batra and Ravisankar (2000) reveals that this is a good approximation of the deformations occurring in the central 75% of the thickness of the plate. In rectangular Cartesian coordinates and in the absence of body forces and sources of internal

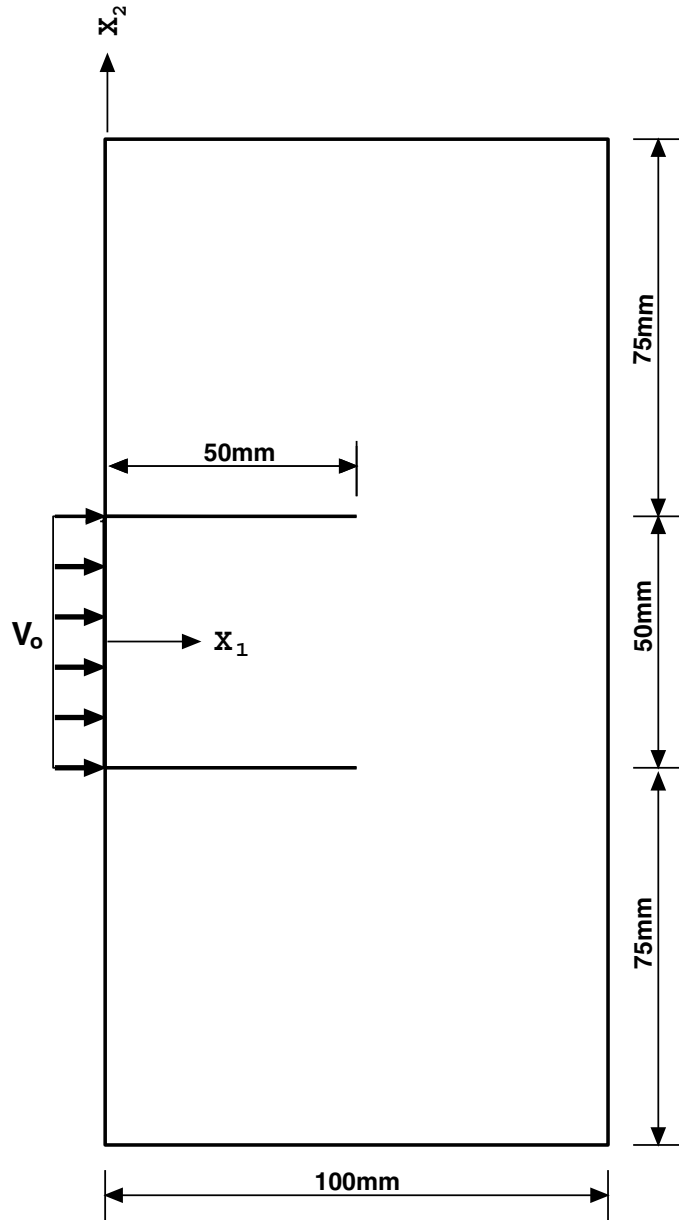


Figure 1. A schematic sketch of the problem studied.

energy, equations governing the deformations of the plate are

$$(\rho J(1 - f))' = 0, \quad (1)$$

$$\rho_0(1 - f_0)\dot{\mathbf{v}} = \text{Div } \mathbf{T}, \quad (2)$$

$$\mathbf{T}\mathbf{F}^T = \mathbf{F}\mathbf{T}^T, \quad (3)$$

$$\rho_0(1 - f_0)\dot{e} = -\text{Div } \mathbf{Q} + \text{tr}(\mathbf{T}\dot{\mathbf{F}}^T). \quad (4)$$

Here ρ is the present mass density, f the porosity, \mathbf{v} the velocity of a material point \mathbf{X} presently occupying the place \mathbf{x} , $\mathbf{F} = \partial \mathbf{x} / \partial \mathbf{X}$, $J = \det \mathbf{F}$, \mathbf{T} the first Piola–Kirchhoff stress tensor, e the

specific internal energy, \mathbf{Q} the heat flux per unit area in the reference configuration, Div the divergence operator with respect to coordinates in the reference configuration, a superimposed dot indicates the material time derivative, tr is the trace operator and \mathbf{F}^T equals the transpose of \mathbf{F} . A subscript 0 on a quantity indicates its value in the reference configuration.

We assume that the plate material is homogeneous and isotropic and use the following constitutive relations to model its thermoviscoplastic response.

$$\dot{\boldsymbol{\sigma}} - \boldsymbol{\Omega}\boldsymbol{\sigma} + \boldsymbol{\sigma}\boldsymbol{\Omega} = \frac{E(1-f)}{(1+\nu)}\mathbf{D}^e + \frac{\nu E(1-f)}{(1+\nu)(1-2\nu)}(\text{tr } \mathbf{D}^e)\mathbf{1}, \quad (5)$$

$$\mathbf{D}^e = \mathbf{D} - \mathbf{D}^p - \alpha\dot{\boldsymbol{\theta}}\mathbf{1}, \quad 2\mathbf{D} = \text{grad } \mathbf{v} + (\text{grad } \mathbf{v})^T, \quad 2\boldsymbol{\Omega} = \text{grad } \mathbf{v} - (\text{grad } \mathbf{v})^T, \quad (6)$$

$$\mathbf{D}^p = \frac{(1-f)\sigma_e\dot{\epsilon}^p}{\text{tr}(\boldsymbol{\sigma}\mathbf{N}^T)}\mathbf{N}, \quad \mathbf{N} = \frac{\partial\Phi}{\partial\boldsymbol{\sigma}}, \quad (7)$$

$$\Phi \equiv \frac{3}{2}\frac{\text{tr}(\mathbf{s}\mathbf{s}^T)}{\sigma_e^2} + 2f^*q_1 \cosh\left(\frac{q_2\text{tr } \boldsymbol{\sigma}}{2\sigma_e}\right) - 1 - q_1^2 f^{*2} = 0, \quad (8)$$

$$\mathbf{s} = \boldsymbol{\sigma} - \frac{1}{3}(\text{tr } \boldsymbol{\sigma})\mathbf{1}, \quad (9)$$

$$\dot{\epsilon}^p = g(\sigma_e, \epsilon^p, \theta), \quad (10)$$

$$f^* = \begin{cases} f & \text{if } f \leq f_c, \\ f_c + \left(\frac{f_u - f_c}{f_f - f_c}\right)(f - f_c) & \text{otherwise,} \end{cases} \quad (11)$$

$$\dot{f} = (1-f)\text{tr } \mathbf{D}^p + \frac{f_2\dot{\epsilon}^p}{s_2\sqrt{2\pi}}\exp\left(-\frac{1}{2}\left(\frac{\epsilon^p - e_N}{s_2}\right)^2\right), \quad (12)$$

$$\mathbf{q} = -\kappa\left(1 - \frac{3}{2}f\right)\text{grad } \theta, \quad (13)$$

$$\dot{c} = c\dot{\theta} + \text{tr}(\boldsymbol{\sigma}\mathbf{D}^e + \alpha\dot{\boldsymbol{\theta}}\boldsymbol{\sigma}), \quad (14)$$

where

$$\mathbf{T} = J\boldsymbol{\sigma}(\mathbf{F}^{-1})^T, \quad \mathbf{Q} = J(\mathbf{F}^{-1})\mathbf{q}. \quad (15)$$

Here $\boldsymbol{\sigma}$ is the Cauchy stress tensor that is related to the first Piola-Kirchhoff stress tensor by eqn. (15)₁, $\boldsymbol{\Omega}$ the spin tensor, E Young's modulus, ν Poisson's ratio, α the coefficient of thermal expansion, \mathbf{D} the strain-rate tensor, $\dot{\epsilon}^p$ the effective plastic strain-rate, \mathbf{q} the heat flux per unit area in the current configuration, κ the thermal conductivity, and c the specific heat. Other parameters characterizing the material are q_1 , q_2 , f_2 , s_2 , e_N , f_c and f_u . Equation (5) is the constitutive relation for a hypoelastic material and its left-hand side represents the Jaumann derivative of $\boldsymbol{\sigma}$.

The frame-indifference of $\boldsymbol{\sigma}$ implies that \mathbf{N} and \mathbf{D}^p are frame-indifferent (cf., Equation (7)) and hence \mathbf{D}^e is frame-indifferent. Therefore Equation (5) is frame-indifferent. The factor $(1-f)$ on the right-hand side of Equation (5) accounts for the degradation of the material strength due to the evolution of the porosity; this was also considered by Passman and Batra (1984) and Kobayashi and Dodd (1989). Budiansky (1970), amongst others, has given the dependence of the material properties upon f for a macroscopically isotropic composite consisting of a random dispersion of approximately spherical voids in a matrix material. These relations are

more involved than the simple reduction of Young's modulus and the bulk modulus by $(1 - f)$. Equation (8) is the yield function proposed by Gurson (1977) and subsequently modified by Tvergaard (1981). Equations $(7)_2$ and $(7)_1$ follow from the assumptions that \mathbf{D}^p is along the outward normal \mathbf{N} to the yield surface $\Phi = 0$, and the plastic working $tr(\boldsymbol{\sigma}\mathbf{D}^p)$ equals $(1 - f)\sigma_e\dot{\epsilon}^p$. The thermoviscoplastic relations described by equation (10) will be discussed below. The expression (11) for f^* was proposed by Tvergaard and Needleman (1984) so that the computed results matched well with the test findings for the cup-cone fracture in a round tensile bar. They suggested the values $f_c \simeq 0.15$ and $f_f \simeq 0.25$.

The first term on the right-hand side of Equation (12) gives the growth of voids due to plastic dilatation, and the second term, proposed by Chu and Needleman (1980) equals the plastic strain controlled nucleation of voids. In Equation (12), s_2 is the standard deviation of the normal distribution, f_2 the volume fraction of voids that would be nucleated if the deformation continued indefinitely, and e_N the plastic strain at which the void nucleation rate is maximum. Experimental studies of LeRoy (1978) and Fisher (1980) on spheroidized carbon steel reveal that a void perfusion strain exists at which the nucleation rate of voids is maximum; this strain can be taken as e_N . Perzyna (1986) has employed a different evolution equation for f . Equation (13) is the Fourier law of heat conduction. Budiansky (1970) proposed that the thermal conductivity of a porous material equals $(1 - (3/2)f)$ of that for the matrix. Nearly all of the thermophysical material parameters may depend upon the temperature. However, such dependencies have been ignored for the sake of simplicity.

For the initial conditions we take

$$\boldsymbol{\sigma}(\mathbf{x}, 0) = \mathbf{0}, \quad f(\mathbf{x}, 0) = f_0, \quad \rho(\mathbf{x}, 0) = \rho_0, \quad \mathbf{v}(\mathbf{x}, 0) = \mathbf{0}, \quad \theta(\mathbf{x}, 0) = \theta_0. \quad (16)$$

That is, the plate is initially stress free and is at a uniform temperature θ_0 . All bounding surfaces of the plate including the surfaces of the two notches are assumed to be traction free and thermally insulated. The surface of the plate impacted by the cylindrical rod is taken to be smooth and the normal velocity, v_1 , on it is given by

$$v_1 = \begin{cases} 0.3v_0t, & 0 \leq t \leq 2\mu s, \\ v_0(0.525 + 0.0375t), & 2 \leq t \leq 10\mu s, \\ 0.9v_0, & 10\mu s \leq t < t_s, \\ 0, & t \geq t_s, \end{cases} \quad (17)$$

where v_0 is the speed of the projectile, and t_s equals the time when the projectile separates from the plate. The expression (17) for v_1 is obtained by fitting straight lines to the data of Batra and Ravisankar (2000) who conducted three-dimensional numerical simulations of the problem studied herein with DYNA3D that models the thermoviscoplastic response of the material by the Johnson–Cook relation. Their simulations with a different constitutive relation and also for a steel with a higher value of the yield stress in a quasistatic simple compression test resulted in expression (17) for the normal velocity imparted to the plate particles.

We assume that the plate is made of a HY100 steel and that the material exhibits strain hardening, strain-rate hardening and thermal softening and model these effects by the following four thermoviscoplastic relations.

2.1. LITONSKI–BATRA RELATION

Batra (1988) generalized the one-dimensional relation of Litonski (1977) to equation (18) appropriate for three dimensional deformations.

$$\dot{\varepsilon}^p = \max \left\{ 0, \frac{1}{b} \left[\left(\frac{\sigma_e}{\sigma_0 \left(1 + \frac{\varepsilon^p}{\varepsilon_y}\right)^n (1 - \nu_s \theta)} \right)^{1/m} - 1.0 \right] \right\}. \quad (18)$$

Here σ_0 is the yield stress of the material in a quasistatic simple tension or compression test, parameters b and m characterize the strain-rate hardening of the material, ε_y and n its strain hardening and ν_s its thermal softening. It is evident from Equation (18) that a material point deforms plastically only when $\sigma_e > \sigma_0 \left(1 + \varepsilon^p/\varepsilon_y\right)^n (1 - \nu_s \theta)$ there.

2.2. POWER LAW

Klopp et al. (1985) and Hartley et al. (1987) described the experimental shear stress-shear strain curve during torsional deformations of a steel tube at different strain rates by a power law. Several investigators, e.g. see Needleman and Tvergaard (1995), have used its three-dimensional version (19) obtained by replacing the shear stress and the shear strain by the effective stress and the effective plastic strain respectively.

$$\dot{\varepsilon}^p = \begin{cases} \dot{\varepsilon}_0 \left(\frac{\sigma_e}{\sigma_0}\right)^{1/m} \left(\frac{\varepsilon^p}{\varepsilon_y}\right)^{-n/m} \left(\frac{\theta}{\theta_0}\right)^{-\gamma/m} & \text{if } \sigma_e \geq \sigma_0, \\ 0 & \text{if } \sigma_e < \sigma_0. \end{cases} \quad (19)$$

Here $\dot{\varepsilon}_0$ is a reference strain-rate and the temperature is measured in Kelvin. The viscoplastic response is characterized by material parameters m , n , γ , σ_0 , θ_0 , ε_y and $\dot{\varepsilon}_0$; θ_0 is usually taken as the room temperature in Kelvin and ε_y the plastic strain at the onset of plastic deformations in a simple tension or compression test.

2.3. BODNER–PARTOM RELATION

Plastic deformations are assumed to occur for all values of the effective stress, and the effective plastic strain-rate is given by (e.g., see Bodner and Partom, 1975)

$$\dot{\varepsilon}^p = D_0 \exp \left[-\frac{1}{2} \left(\frac{K^2}{3\sigma_e^2} \right)^n \right], \quad (20)$$

where

$$K = K_1 - (K_1 - K_0) \exp(-m W_p), \quad n = \frac{a}{\theta} + b, \quad (21)$$

$$W_p = \int_0^t \text{tr}(\boldsymbol{\sigma} \mathbf{D}^p) dt. \quad (22)$$

Parameters K_1 , K_0 , D_0 , m , a and b determine the thermoviscoplastic response of the material, and the temperature θ in Equation (21)₂ is measured in Kelvin.

2.4. JOHNSON–COOK RELATION

Based on the test data at moderate values of the strain-rate and at different temperatures, Johnson and Cook (1983) proposed that

$$\dot{\varepsilon}^p = \dot{\varepsilon}_0 \max \left\{ \exp \left[\frac{1}{C} \left(\frac{\sigma_e}{(A + B(\varepsilon^p)^n) \left(1 - \left(\frac{\theta - \theta_0}{\theta_m - \theta_0} \right)^m \right)} - 1 \right) \right], 0 \right\}. \quad (23)$$

The reference strain-rate, $\dot{\varepsilon}_0$, is usually taken as 1/s and θ_m equals the melting temperature of the material. When $\theta = \theta_m$, the material behaves as a perfect fluid.

3. Numerical solution of the governing equations

Because of the relation (15)₁ between \mathbf{T} and $\boldsymbol{\sigma}$ and the constitutive relation (5), the balance of moment of momentum (3) is identically satisfied. The present mass density, ρ , can be computed from Equation (1) if the deformation and current value of the porosity are known. Thus the independent variables are \mathbf{X} and t , and the dependent variables are \mathbf{x} , f and θ . Equations (2) and (4) are second-order nonlinear hyperbolic and parabolic partial differential equations (PDEs) for \mathbf{x} and θ ; the two are coupled through the source term in (4) and the dependence of \mathbf{T} upon θ through the thermoviscoplastic relation (10). There is no easy way to write eqns. (2) and (4) in terms of \mathbf{x} and θ since \mathbf{T} is given by (15)₁ and $\boldsymbol{\sigma}$ is a solution of the ordinary differential equation (5) which involves \mathbf{D}^p and θ through (6)₁.

The problem formulated above is numerically solved by the finite element method. The domain of study is divided into constant strain triangular (CST) elements. The Galerkin approximation of equations (2) and that obtained by substituting from (13), (14) and (15)₂ into (4) yields a coupled set of ordinary differential equations for nodal values of the two components of the velocity and the temperature. Equations (1), (5), (10) and (12) are integrated at the centroid of an element. The value of σ_e is computed from the yield function (8) after $\boldsymbol{\sigma}$ and hence \mathbf{s} have been determined. Thus, for the plane strain problem, the number of unknowns and the number of coupled nonlinear ordinary differential equations (ODEs) to be integrated equal 3 (nodes) + 7 (elements). These ODEs subject to the prescribed initial conditions are integrated with respect to time t by using the subroutine LSODE (Livermore Solver for Ordinary Differential Equations) included in the package ODEPACK. Because of the storage limitations, we used the nonstiff option in LSODE with $MF = 10$, $ATOL = RTOL = 10^{-6}$. The ODEs are integrated by the Adams method; the order of the method and the time step size are adaptively adjusted to solve the ODEs within the prescribed tolerance. In LSODE, the value of the parameter MF selects the method, and the values of ATOL and RTOL equal respectively the absolute and the relative tolerances on the solution variables.

We modified the computer code developed by Batra and Jin (1994) for the analysis of plane strain thermomechanical deformations of a viscoplastic body with the Litonski–Batra relation. The modifications include the incorporation of the Bodner–Partom and the Johnson–Cook relations and the power law. Batra and Jin (1994) also multiplied Equations (1), (5), (10) and (12) by a test function, integrated the resulting equations over the domain of study and obtained ODEs for nodal values of the mass density, porosity and four components of the stress tensor. Here these equations are integrated at the centroids of elements thereby reducing

the total number of unknowns. Recall that for a CST element, the deformation gradient and the strain-rate etc. are constants over the element. For the Johnson–Cook thermoviscoplastic relation results computed with the current code were found to be quite close to those obtained with DYNA2D until the time the deformations localized into a narrow band in the prenotched plate. Whereas our code accounts for heat conduction, thermal expansion and the evolution of the porosity, these are ignored in DYNA2D. The DYNA2D employs the 4-node quadrilateral element with one-point integration rule, an hour-glass control, a lumped mass matrix, and the explicit central-difference method to integrate the ODEs and is computationally very efficient. In our code, the lumped mass matrix for the CST elements is obtained by the row sum technique.

Results computed with DYNA2D for the prenotched plate with the Jaumann and the Green-Naghdi stress rates on the left-hand side of Equation (5) were found to be identical with each other. It is primarily because the plastic strain-rates at points near the notch tip are significantly larger than the elastic strain-rates and the latter appear in the right-hand side of Equation (5).

4. Values of material parameters

Batra and Kim (1990) used the aforesaid four thermoviscoplastic relations to study the initiation and development of shear bands in a viscoplastic block made of a HY-100 steel and deformed in simple shear. They simulated the dynamic torsional tests of Marchand and Duffy (1988) on thin-walled HY-100 steel tubes as a simple shearing problem, determined the values of material parameters by solving an initial-boundary-value problem and adjusted the values of material parameters till the computed shear stress-shear strain curve closely matched with the experimental curve of Marchand and Duffy. During the iterative process of finding the appropriate values of material parameters, the value of the quasistatic yield stress of the material was kept the same as that provided by Marchand and Duffy's tests and that of the strain hardening exponent was kept close to the value Marchand and Duffy found by curve fitting their test data. The values of other material parameters are not uniquely determined since the underlying initial-boundary-value problem need not have a unique solution. Batra and Kim's values of material parameters were suitably modified to account for three-dimensional deformations of the viscoplastic body.

Values assigned to material parameters in the four thermoviscoplastic relations are listed below.

- (a) Litonski–Batra
 $v_s = 0.00185 \text{ }^\circ\text{C}$, $\varepsilon_y = 0.007$, $n = 0.107$, $m = 0.0117$, $b = 17320 \text{ s}$.
- (b) Power law
 $\dot{\varepsilon}_0 = 5.77 \times 10^{-5} \text{ s}^{-1}$, $\varepsilon_y = 0.007$, $\theta_0 = 300 \text{ K}$, $m = 0.0117$, $n = 0.107$, $\gamma = -0.27$.
- (c) Bodner–Partom
 $a = 1200 \text{ K}$, $b = 0$, $K_1 = 2950 \text{ MPa}$, $K_0 = 2937 \text{ MPa}$, $m = 3510 \text{ MPa}$, $D_0 = 1.732 \times 10^8 \text{ s}^{-1}$.
- (d) Johnson–Cook
 $A = 316 \text{ MPa}$, $B = 1067 \text{ MPa}$, $n = 0.107$, $\theta_m = 1500 \text{ K}$, $\theta_0 = 300 \text{ K}$, $m = 0.7$, $C = 0.0277$, $\dot{\varepsilon}_0 = 3300 \text{ s}^{-1}$.

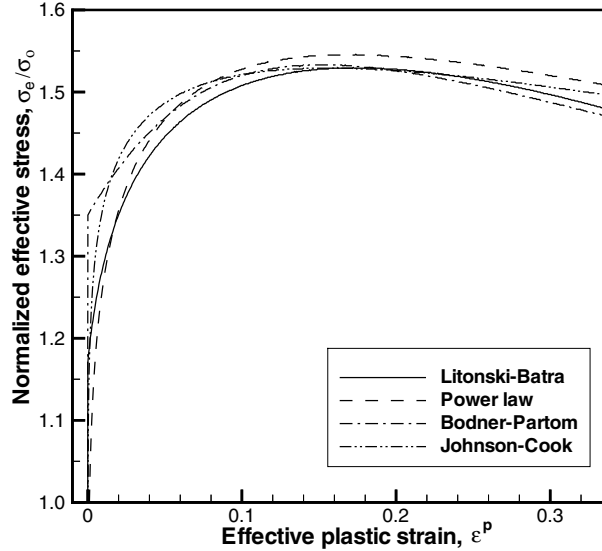


Figure 2. Effective stress vs. effective plastic strain curves for homogeneous deformations of a block deformed at an average strain-rate of 3300 s^{-1} .

Values of other material parameters used to compute results are:

$$\begin{aligned} \sigma_0 = 702 \text{ MPa}, \quad \rho_0 = 7860 \text{ kg m}^{-3}, \quad c = 473 \text{ J/kg } ^\circ\text{C}, \quad K = 49.73 \text{ W m}^{-2} \text{ } ^\circ\text{C}, \\ \alpha = 11.5 \times 10^{-6} / ^\circ\text{C}, \quad E = 208 \text{ GPa}, \quad \nu = 0.3, \quad f_2 = 0.04, \quad e_N = 0.3, \\ s_2 = 0.1, \quad q_1 = 1.5, \quad q_2 = 1.0, \quad f_c = 0.15, \quad f_f = 0.25, \quad f_u = 0.667, \quad f_0 = 0.0. \end{aligned} \quad (24)$$

Values of e_N , s_2 , q_1 , q_2 , f_c , f_f , f_u , etc., are for a typical steel. Figure 2 depicts the computed effective stress versus the effective plastic strain curves for homogeneous deformations of a block deformed at a nominal strain-rate of 3300 s^{-1} . It is clear that the four curves are quite close to each other. Note that the expanded scale along the vertical axis magnifies the small differences among the four curves.

5. Computation and discussion of results

Due to the symmetry of the plate and the applied initial and boundary conditions about the x_1 - x_3 plane passing through the centroid of the plate, deformations of only the upper half of the plate are analyzed. For a notch tip radius of 0.15 mm, Figure 3a exhibits the discretization of the domain into three-noded triangular elements, and Figure 3b shows the details of the mesh around the notch tip. There are 40 elements around the notch tip surface and the element size increases gradually as one moves away from this surface. The qualitative and quantitative nature of results computed with a finer mesh was essentially unchanged at points close to the notch tip surface. Results presented below are with a fixed mesh. Computations were stopped when one of the elements abutting the notch tip surface got severely distorted.

For each one of the four thermoviscoplastic relations and for the notch tip radius $r_0 = 0.15 \text{ mm}$, impact speed $v_0 = 20 \text{ m s}^{-1}$ and time $t = 25 \text{ } \mu\text{s}$, Figures 4a, 4b and 4c evince respectively the fringe plots of the effective plastic strain, the normalized maximum principal stress σ_p/σ_0 and the normalized shear stress σ_{12} in a small region around the notch tip. The results are qualitatively similar for the four thermoviscoplastic relations. In each case, the

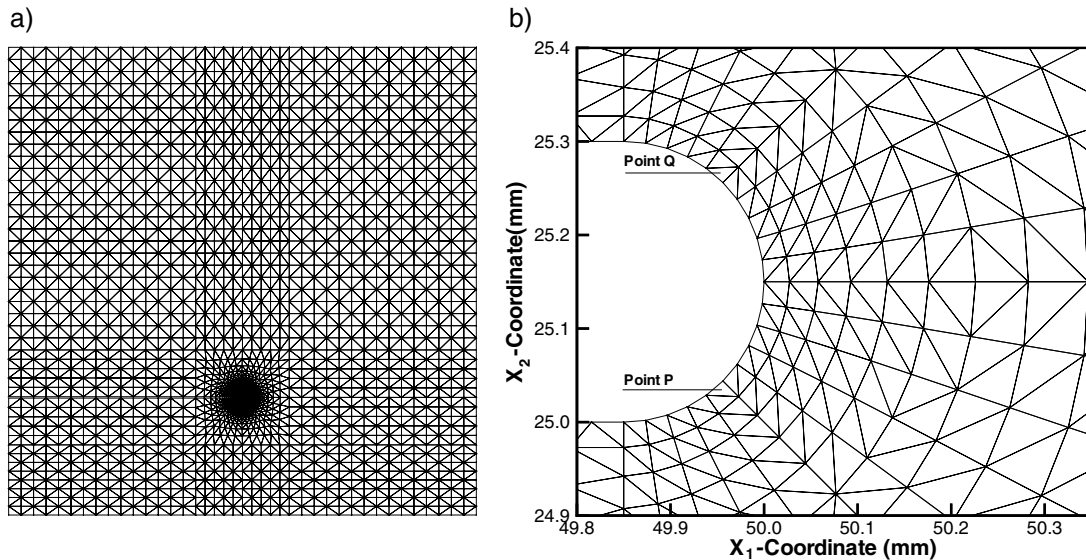


Figure 3. (a) Finite element discretization of the problem domain. (b) Details of the finite element mesh in the region surrounding the notch tip.

maximum effective plastic strain occurs at a point on the lower surface of the notch tip and its value equals at least 0.30. The intensely deformed region is nearly of the same size and is likewise oriented. Small kinks in the lower part of the bounding surface of the notch tip are due to the severe distortions of the elements in that region. These plots suggest that the ductile failure will initiate from a point on the lower part of the notch tip surface. A comparison of the bounding surface of the undeformed notch shown in Figure 3b with that of the deformed one in Figure 4a reveals that the notch surface is not symmetrically deformed about its center-line. This is to be expected since the applied load is asymmetric about the centerline of the notch. Points on the lower traction free surface of the notch move to the right, i.e., in the direction of the prescribed velocity while those on the upper surface remain essentially stationary; e.g., see the velocity plots given in Figure 4 of Batra and Gummalla (2000). The velocity plots for the results computed herein were similar to that shown in Figure 4 of Batra and Gummalla, and are therefore omitted. This relative movement of material particles induces stretching and hence tensile stresses in the region adjoining the upper part of the notch tip surface; this is depicted in Figure 4b. For each one of the four thermoviscoplastic relations, the maximum principal tensile stress occurs at a point situated approximately 0.09 mm above the upper surface of the notch tip and equals almost $2.5\sigma_0$. The principal stress is compressive in the region near the lower surface of the notch tip where the effective plastic strain is high. These observations are consistent with the results of previous investigations of the problem by Needleman and Tvergaard (1995), Zhou et al. (1996b), Batra and Nechitailo (1997), Batra and Gummalla (2000) and Batra and Ravisankar (2000), and suggest that a brittle failure will ensue from a point on the upper surface of the notch tip. Needleman and Tvergaard used a power law type viscoplastic relation, Zhou et al. modeled thermal softening by an exponential function, and the other three investigations employed the Johnson–Cook relation. Needleman and Tvergaard's results as well as those of the present study suggest that the consideration of the porosity does not change the qualitative and the quantitative nature of results. The maximum value of the porosity computed at any point in the plate before an element got severely distorted equalled

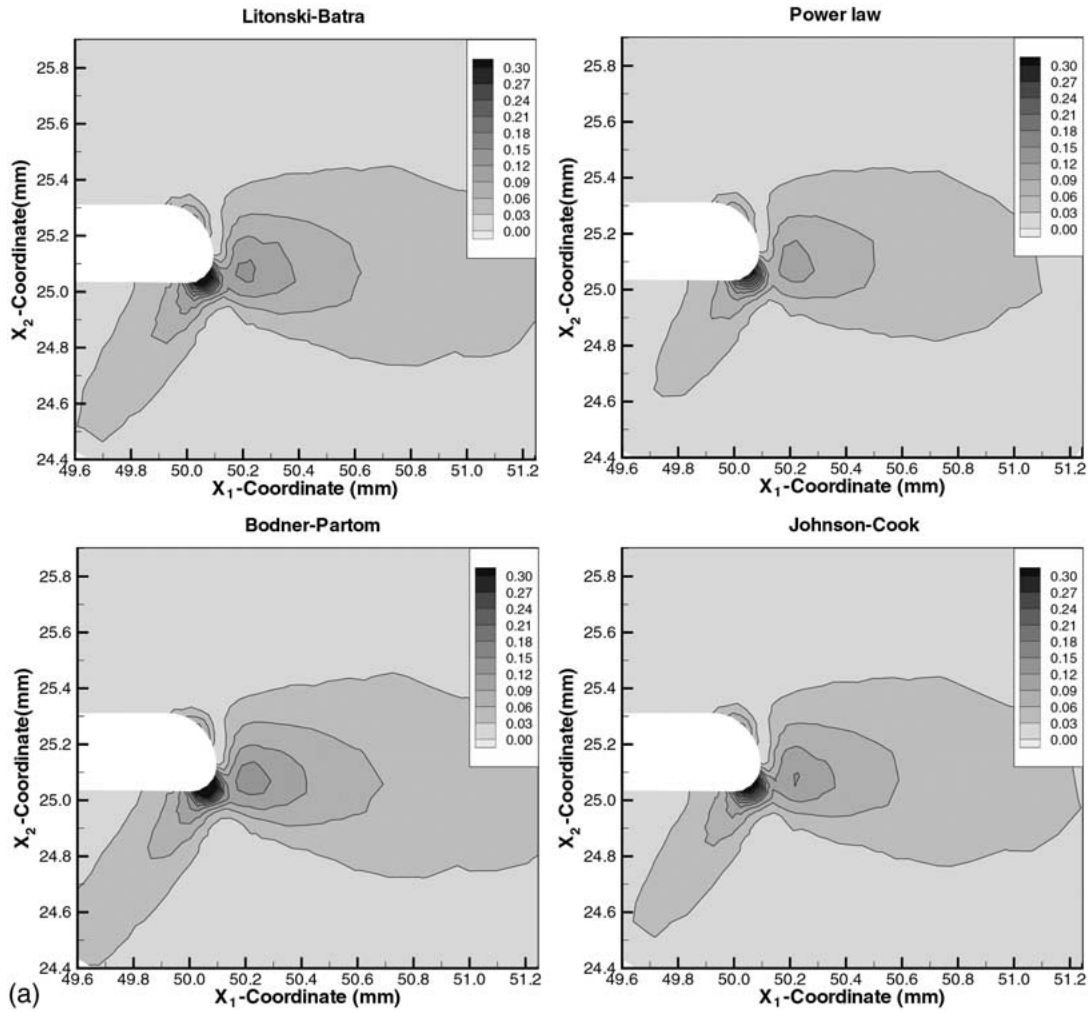


Figure 4. For the four thermoviscoplastic relations, fringe plots in a small region surrounding the surface of the notch tip, of (a) the effective plastic strain, (b) the normalized maximum principal stress, and (c) the normalized shear stress σ_{12} .

2.75%. One reason could be that as soon as the effective plastic strain at a point becomes large enough for the voids to nucleate, the mesh gets severely distorted and computations need to be ceased. Our attempts to adaptively refine the mesh resulted in noticeable oscillations in the evolution of the effective stress at a point and thus were abandoned. These oscillations were due to the transfer of the data from the old mesh to the new one. In the plane strain transient thermomechanical deformations of a viscoplastic block studied by Batra and Jin (1994) and by Batra and Ko (1992), these oscillations were not large enough to significantly affect subsequent computations. However, for the present problem, points on the notch surface moved noticeably and attempts to smoothen the adaptively generated mesh did not improve the situation. Results presented herein are, therefore, with a fixed mesh.

The fringe plots of the normalized shear stress σ_{12} depicted in Figure 4c indicate that for each one of the four viscoplastic relations the maximum shear stress occurs in a region directly ahead of the notch tip. Chen and Batra (1999) scrutinized the asymptotic deformation

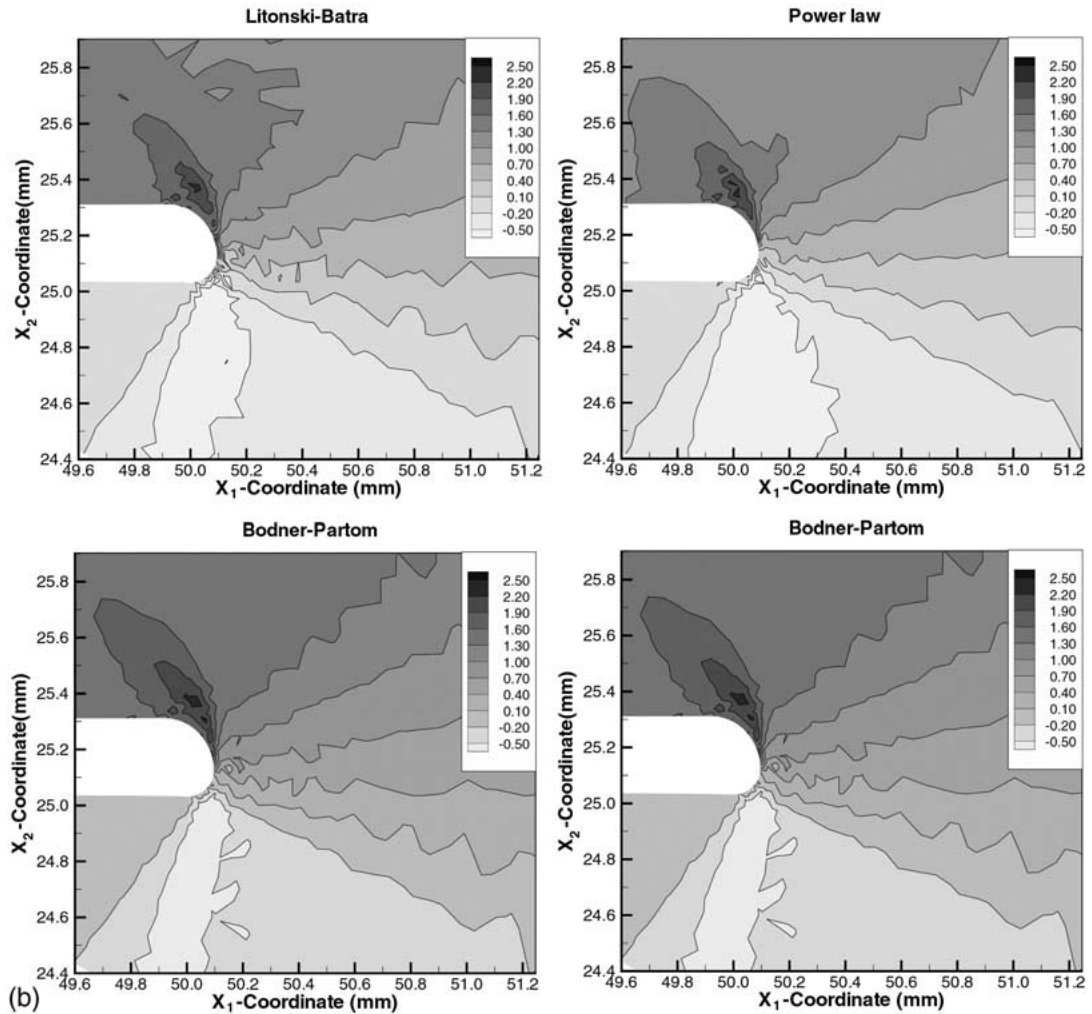


Figure 4. Continued.

fields around a shear band tip propagating at a uniform velocity in a thermoviscoplastic body undergoing plane strain deformations. They modeled the shear band as a singular surface and observed that the jump in the shear stress across the singular surface acted as a driving force for the propagation of a shear band. Hence in the present problem, a shear band will propagate predominantly along the axis of the notch and a secondary band may propagate in a direction making an angle of about 130° clockwise from the axis of the notch. The existence of a secondary shear band is evidenced by the two lobes of high effective plastic strain in Figure 4a. Experimental observations of Kalthoff et al. (1987), Mason et al. (1994) and Zhou et al. (1996a) indicate that a shear band propagates nearly along the axis of the notch. Thus the direction of propagation of a shear band predicted by each one of the four thermoviscoplastic relations is close to that observed experimentally.

In an attempt to quantitatively delineate the differences, if any, in the results predicted by the four thermoviscoplastic relations we have plotted in Figures 5a and 5b the time histories of the normalized effective stress, the effective plastic strain, the normalized maximum principal stress and the temperature at points P and Q . Points P and Q , shown in Figure 3b, are at

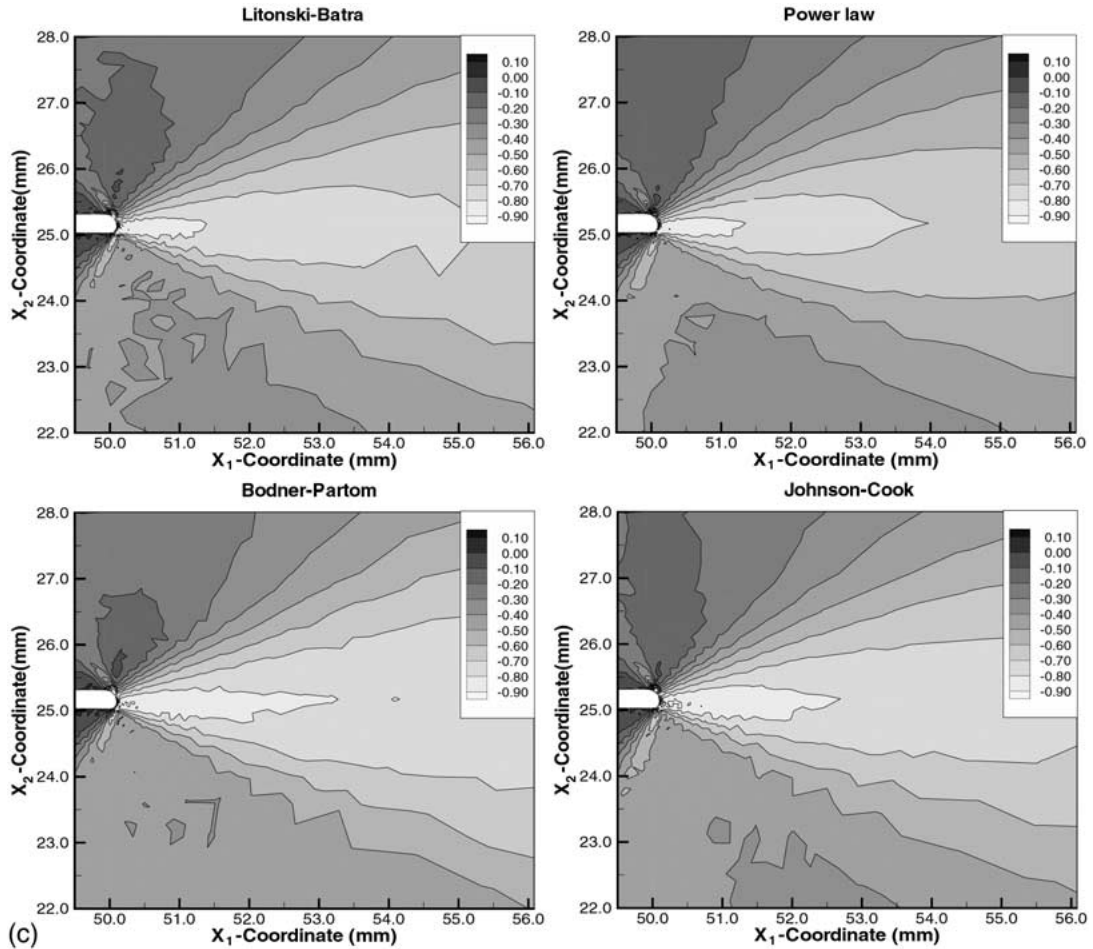


Figure 4. Continued.

the centroids of elements abutting the notch tip surface, and lines OP and OQ are inclined respectively at 45° clockwise and 45° counterclockwise to the axis of the notch. Point O coincides with the centroid of the notch tip. For the values of material parameters used herein, the dilatational wave speed equals about $5.8 \text{ mm } \mu\text{s}^{-1}$. The effective stress begins to grow at points around the notch tip soon after the loading wave arrives there at $t \simeq 8 \text{ } \mu\text{s}$, and the 200 mm long striker rod separates from the prenotched plate at $t_s \simeq 32 \text{ } \mu\text{s}$. Once the effective stress at a point exceeds the dynamic yield stress of the material, the material point starts deforming plastically. The initial effective plastic strain-rate at point P or Q computed with each one of the four thermoviscoplastic relations is virtually the same even though the effective stress is a little different. At $t \simeq 14 \text{ } \mu\text{s}$, the effective plastic strain-rate computed at point Q with the four constitutive relations begins to differ; the power law gives the lowest value and the Bodner–Partom relation the highest value. Each one of the four constitutive relations gives an effective plastic strain-rate at point P which is of the order of 10^4 s^{-1} . Results computed at point Q with the four thermoviscoplastic relations are closer to each other than those at point P . During the time interval $0 \leq t \leq 30 \text{ } \mu\text{s}$, the maximum effective plastic strain induced at point Q is less than one-half of that at point P . However, the magnitude of the maximum

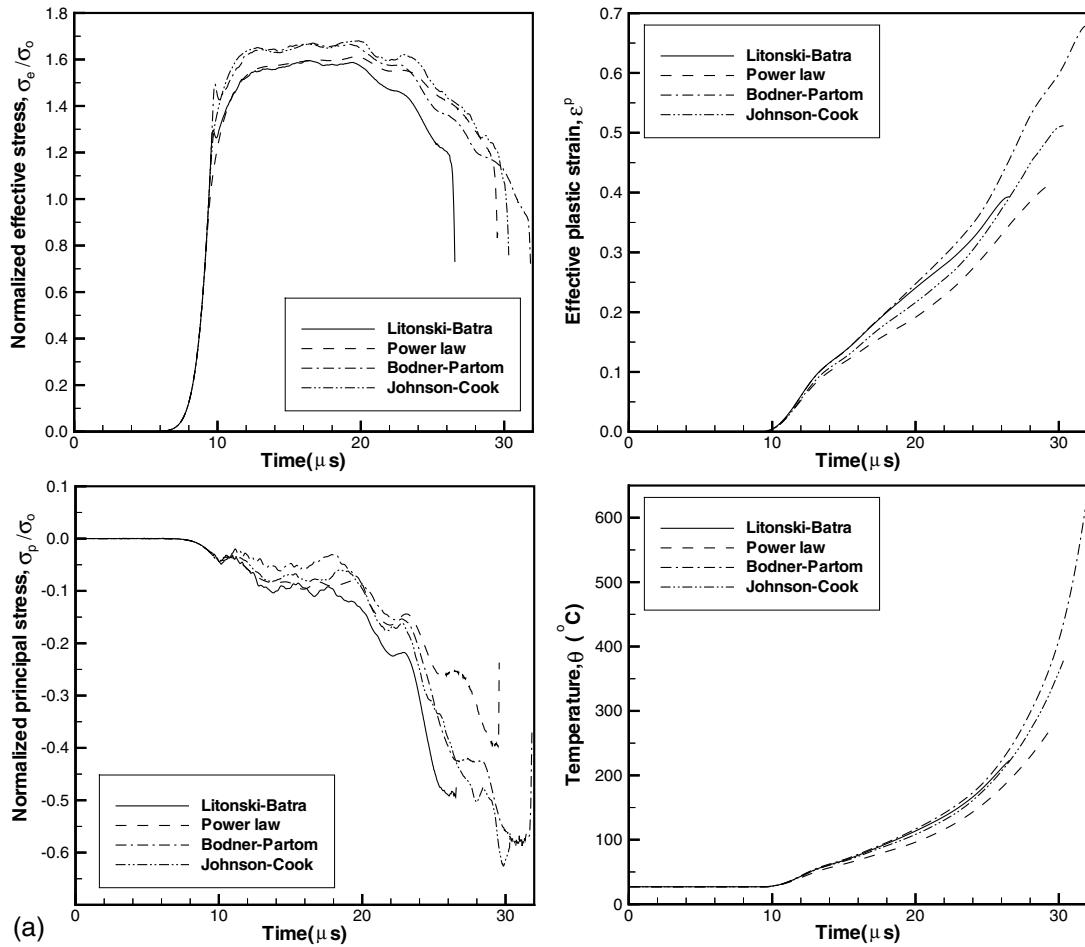


Figure 5. (a) For the four thermoviscoplastic relations, time histories at the point P on the notch surface that is located at 45° clockwise from the axis of the notch of (i) the normalized effective stress, (ii) the effective plastic strain, (iii) the normalized maximum principal stress, and (iv) the temperature. (b) For the four thermoviscoplastic relations, time histories at the point Q on the notch surface that is located at 45° counterclockwise from the axis of the notch of (i) the normalized effective stress, (ii) the effective plastic strain, (iii) the normalized maximum principal stress, and (iv) the temperature.

tensile principal stress at point Q is nearly three times that of the maximum compressive principal stress at point P . The temperature rise at point P is approximately three times as large as that at point Q . Note that the maximum principal tensile stress occurs in an element away from the notch surface. The computed temperature is highest for the Bodner-Partom relation and least for the power law.

Figure 6 exhibits at $t = 25 \mu\text{s}$ the angular variation of the normalized maximum principal stress, the effective plastic strain, the temperature and the porosity at the centroids of elements abutting the notch tip surface; positive angles are measured counterclockwise from the axis of the notch. Only a small portion of the material adjacent to the notch tip surface and lying in the reference configuration within the angular region $-70^{\circ} \leq \phi \leq -40^{\circ}$ is intensely deformed. The location and the size of the intensely deformed region is the same for each one of the

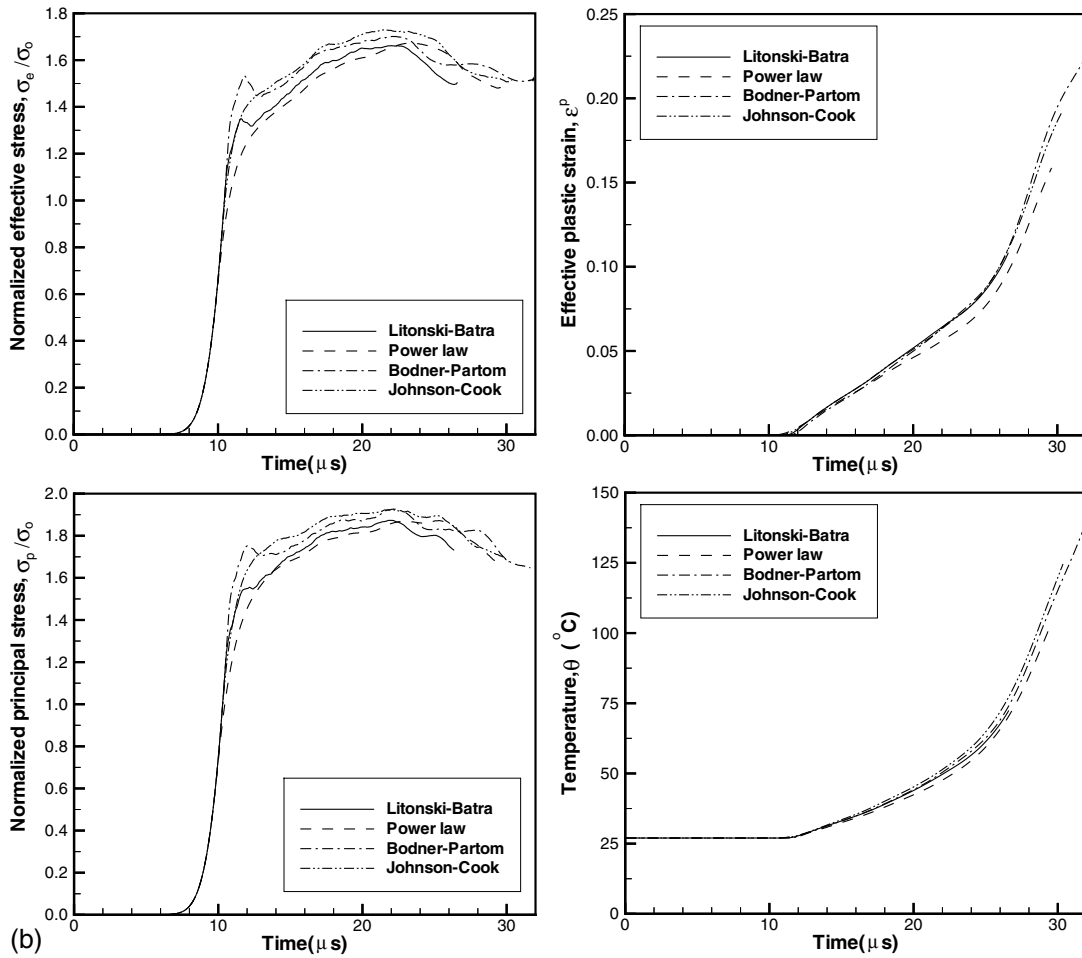


Figure 5. Continued.

four constitutive relations but the maximum effective plastic strain induced and the porosity evolved are different.

We note that the deformations of material points close to the surface of the notch tip do not correspond to that of simple shearing. The analytical work of Lee and Freund (1990) based on the assumptions of plane strain deformations and linear elasticity shows that the mode mixity equals -0.25 till waves reflected from the unloaded edge of the plate arrive at the notch tip. This suggests that both mode-I and mode-II deformations occur at points near the notch tip. Batra and Ravisankar's (2000) numerical simulation of the three-dimensional problem reveals that there is also a noticeable K_{III} component of deformation at points on the front or back surface of the plate that are close to the notch tip surface. Our computed results for the prenotched plate indicate that the four thermoviscoplastic relations studied herein predict different results for mixed mode deformations even though they were calibrated to give very close effective stress vs. effective strain curves in simple shearing. Batra and Chen (2001) found that even in simple shearing deformations of a thermoviscoplastic block, these four thermoviscoplastic relations predicted different values of the instability strain, shear band initiation strain, shear band width, and the spacing between adjacent shear bands.

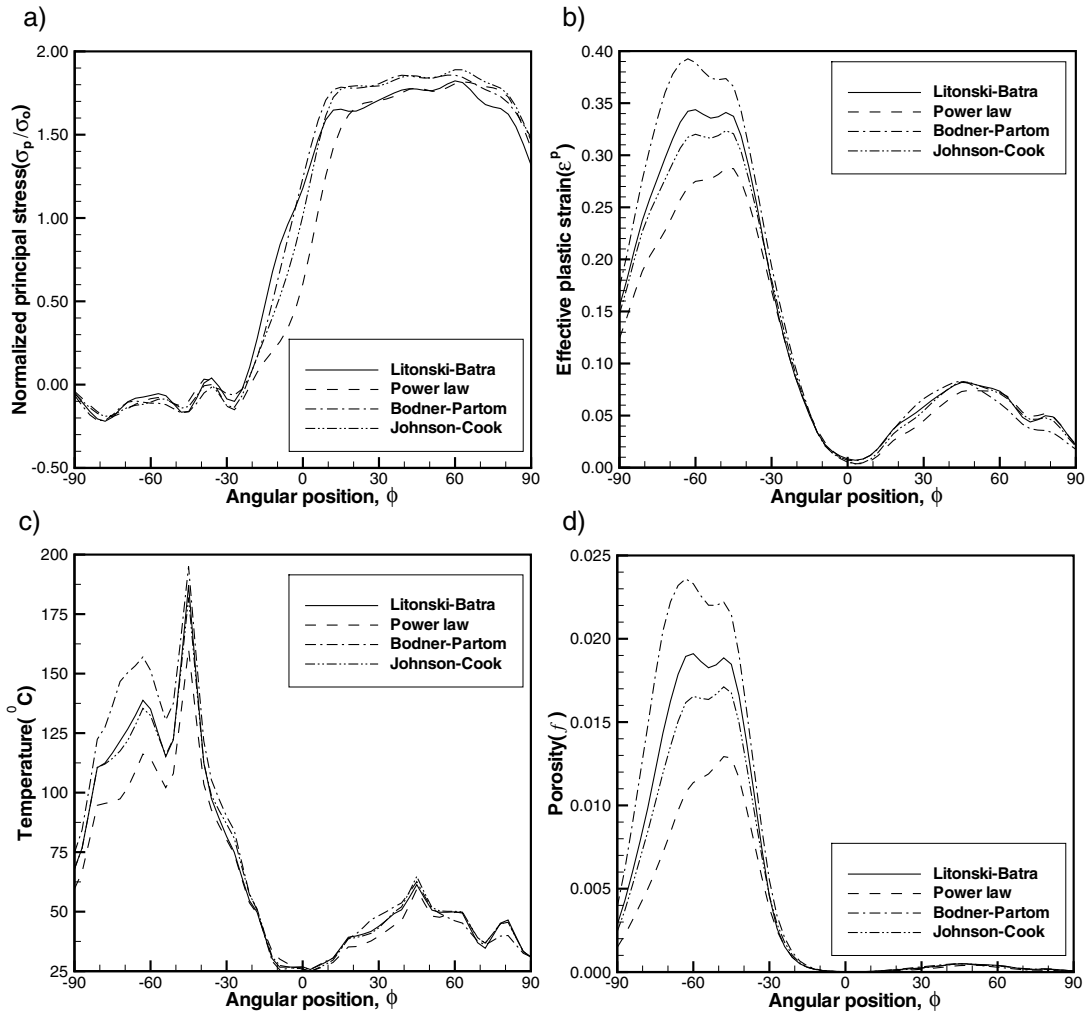


Figure 6. At $t = 25 \mu\text{s}$, the angular variation of the normalized maximum principal stress, the effective plastic strain, the temperature and the porosity at the centroids of elements abutting the notch tip surface.

6. Failure mode transition speed

In order to determine the speed at which the failure mode changes from brittle to ductile or vice-versa, one needs to define a criterion for the initiation of a failure mode. It is generally believed that a brittle failure ensues at a point when the maximum principal tensile stress, σ_p , there attains a critical value. Ritchie et al. (1973) have proposed that the brittle failure occurs when $\sigma_p/\sigma_0 = 3.0$ over a certain length which is characteristic of the microstructure of the material and typically equals the grain diameter. Since the stresses are constant over the CST element, the size of the smallest element exceeds $23 \mu\text{m}$, and the grain diameter is generally less than $23 \mu\text{m}$, therefore the condition of the principal stress exceeding a critical value over a certain length is easily met. However, tensile experiments of Hendrickson et al. (1958) on prenotched steel specimens at nominal stress rates of about 1 to 10^4 MPa s^{-1} show that the transition from brittle to ductile failure occurs at $\sigma_p/\sigma_0 \simeq 2.34$; the steel had a yield strength of 705 MPa . This value of σ_p/σ_0 was found to be essentially independent of the

temperature and the rate of loading. In their numerical simulation of the Kalthoff experiment, Zhou et al. (1996b), Batra and Gummalla (2000) and Batra and Ravisankar (2000) presumed that the brittle failure initiates when $\sigma_p/\sigma_0 = 3.0$, 2.0 and 2.0, respectively. For the configurations and impact speeds numerically simulated by Batra and Ravisankar and Zhou et al., no brittle failure initiated at any point in the prenotched plate. Here, based on the test data of Hendrickson et al. (1958) we assume that the brittle failure initiates at a material point when $\sigma_p/\sigma_0 = 2.34$ there.

Batra and Kim (1992) have numerically studied the initiation and development of shear bands in twelve materials deformed in simple shear. A material defect was modeled by assuming that the thickness of the block varied sinusoidally with the smallest thickness occurring at the block's center. Based on their numerical experiments, Batra and Kim (1992) proposed that a shear band initiates at a point when the shear stress there has dropped to 90% of its maximum value and the material point is deforming plastically; this and other works have been summarized by Batra (1998). We recall that in their torsional tests on thin-walled HY-100 steel tubes, Marchand and Duffy (1988) regarded the initiation of a shear band as synonymous with the sudden drop in the torque required to twist the tube. They reported the maximum shear strain of 20 within a shear band. Mason et al. (1994) measured an effective plastic strain of 1.0 in a shear band formed in a C-300 maraging steel, and Zhou et al. (1996a) measured the time histories of the temperature at a point on the front surface of a prenotched C-300 maraging steel plate and located about 6-mm ahead of the notch tip. In their numerical simulations of the Kalthoff experiment, Zhou et al. (1996b) and Batra and Gummalla (2000) assumed that a shear band initiates when the effective plastic strain at a point equals a prespecified value. However, Batra and Ravisankar (2000) regarded the shear band to initiate at a point when the effective stress there has dropped to 90% of its maximum value at that point and the material point is deforming plastically. As shown by Batra and Rattazzi (1997) the time of initiation of a shear band and the computed shear band speed depend upon the criterion used to characterize the initiation of a shear band. Thus the values of the impact speed given below at which the failure mode transitions from the brittle failure to the ductile failure as signified by the initiation of a shear band depend upon the criteria employed for the initiation of the two failure modes. Our simulations did not include the opening of a crack. Once a crack forms, the domain of study of the problem changes.

For the four thermoviscoplastic relations studied, Figure 7 shows the variation of the time of initiation of the two failure modes with the impact speed. The depicted curves were obtained by the least squares fit of quadratic polynomials to the computed data points. The brittle failure usually initiated at a point situated nearly 0.09 mm from the surface of the notch tip and the line joining it with the center of the notch tip made an angle, in the reference configuration, of about 60° counterclockwise with the axis of the notch. The ductile failure generally originated from a point on the notch surface; the line joining it with the center of the notch tip made an angle, in the reference configuration, of approximately 45° clockwise with the axis of the notch. For a notch tip radius of 0.15 mm, the impact speed, v_0 , at which the failure mode transitions from brittle to ductile equals 13.5, 18.5, 19.3 and 22.9 m s⁻¹, respectively, for the Litonski–Batra, the power law, the Bodner–Partom and the Johnson–Cook relations. Thus the four thermoviscoplastic relations predict different values of the transition speed.

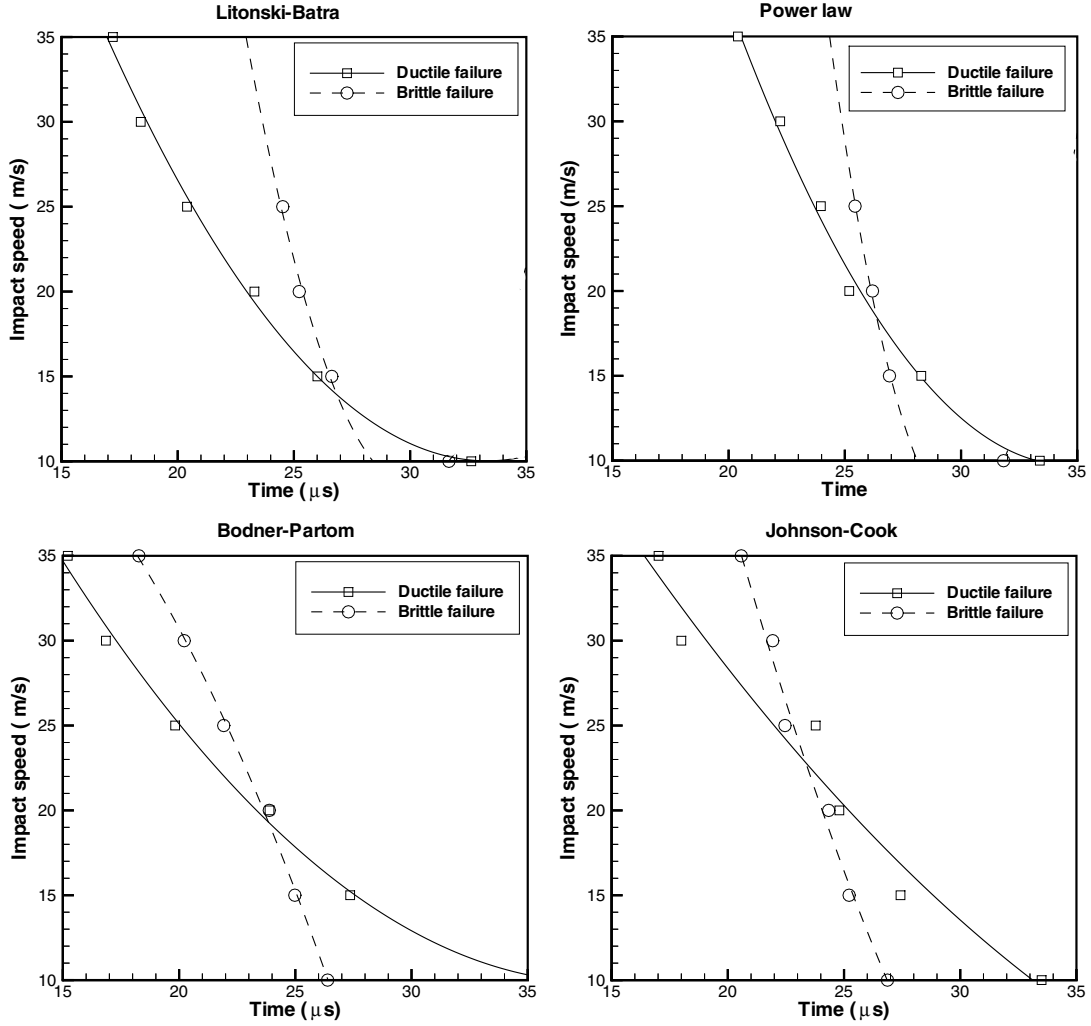


Figure 7. For the four thermoviscoplastic relations, the dependence of the times of initiation of the brittle and ductile failures upon the impact speed v_0 .

7. Effect of notch tip radius

Having established above that all four thermoviscoplastic relations give qualitatively similar results, we use only the Bodner–Partom relation to investigate the effect of the notch tip radius on the speed of transition from the brittle failure to the ductile failure. Figure 8a evinces the straight line obtained by the least squares fit to the computed values of $\ln v_{cr}$ and $\ln r_0$ for $r_0 = 0.15, 0.20$ and 0.25 mm; v_{cr} and r_0 have been normalized by 1 m s^{-1} and 1 m , respectively. From the values of the slope and the y -intercept, we conclude that for the mild steel being studied

$$v_{cr} = 1179 r_0^{0.4655} \text{ m s}^{-1}, \quad (25)$$

where r_0 is in meters. This compares well with the relation

$$v_{cr} = 1350 r_0^{0.5} \text{ m s}^{-1}, \quad (26)$$

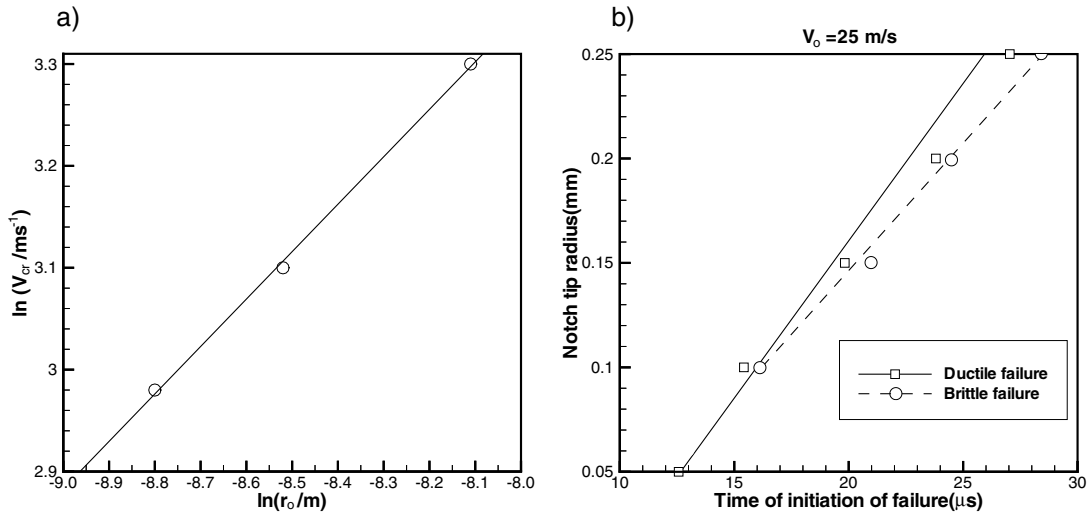


Figure 8. (a) Dependence of the transition speed, v_{cr} , upon the notch tip radius, r_0 , for a mild steel prenotched plate. (b) Effect of the notch tip radius on the times of initiation of the brittle and the ductile failure.

obtained by Kalthoff (2000) based on his test findings. We note that Kalthoff tested prenotched plates made of a high strength steel with $r_0 \geq 0.15 \text{ mm}$. For the mild steel plate studied herein and $10 \leq v_0 \leq 35 \text{ m s}^{-1}$, no brittle failure was observed for $r_0 = 0.05 \text{ mm}$. Also the computed values of v_{cr} for $r_0 = 0.3 \text{ mm}$ did not satisfy the relation (25).

For an impact speed of 25 m s^{-1} , Figure 8b exhibits the least-square fit straight lines to the computed times of initiation of the two failure modes for different values of the notch tip radius, r_0 . Results should not be extrapolated outside the range of values of r_0 considered since these curves suggest that for $r_0 = 0.05 \text{ mm}$, brittle failure will ensue but, as stated above, this failure mode did not ensue in our computations. For $0.1 \leq r_0 \leq 0.25 \text{ mm}$, the time of initiation of the two failure modes increases affinely with an increase in the value of r_0 , and the ductile failure ensues first. We recall that the opening and consequently propagation of a crack has not been simulated. Once a crack opens due to the initiation of either one of the two failure modes, subsequent deformations of the plate will most likely differ noticeably from those computed here, and the difference in the times of initiation of the two failure modes will not necessarily equal that shown in Figure 8b.

For an impact speed of 20 m s^{-1} , Figures 9a and 9b show the time histories of the effective stress and the effective plastic strain at a material point located on the notch tip surface and, in the reference configuration, at an angular position of 45° clockwise from the axis of the notch. As expected, the rate of increase of the effective plastic strain is quite high for $r_0 = 0.05 \text{ mm}$ and it decreases with an increase in the value of r_0 . For $r_0 = 0.05 \text{ mm}$ the effective stress drops rather precipitously soon after it has reached its peak value; the rate of drop of the effective stress becomes more gradual with an increase in the value of r_0 . We assume that $\dot{\epsilon}^p \propto r_0^\beta$ where $\dot{\epsilon}^p$ is the effective plastic strain rate at the point on the notch tip surface that makes in the reference configuration an angle of 45° clockwise with the axis of the notch. The least squares fit straight lines to the computed values of $\ln(\dot{\epsilon}^p / \text{s}^{-1})$ at $t = 10 \mu\text{s}$ and $\ln(r_0/1 \text{ mm})$ provided $\beta = -0.93$ for $v_0 = 20 \text{ m s}^{-1}$ and $\beta = -0.812$ for $v_0 = 35 \text{ m s}^{-1}$. The order of singularity depends not only upon the impact speed but also on the time when $\dot{\epsilon}^p$ is measured. For the Johnson–Cook relation, a different steel, and $v_0 \simeq 28 \text{ m s}^{-1}$, Batra

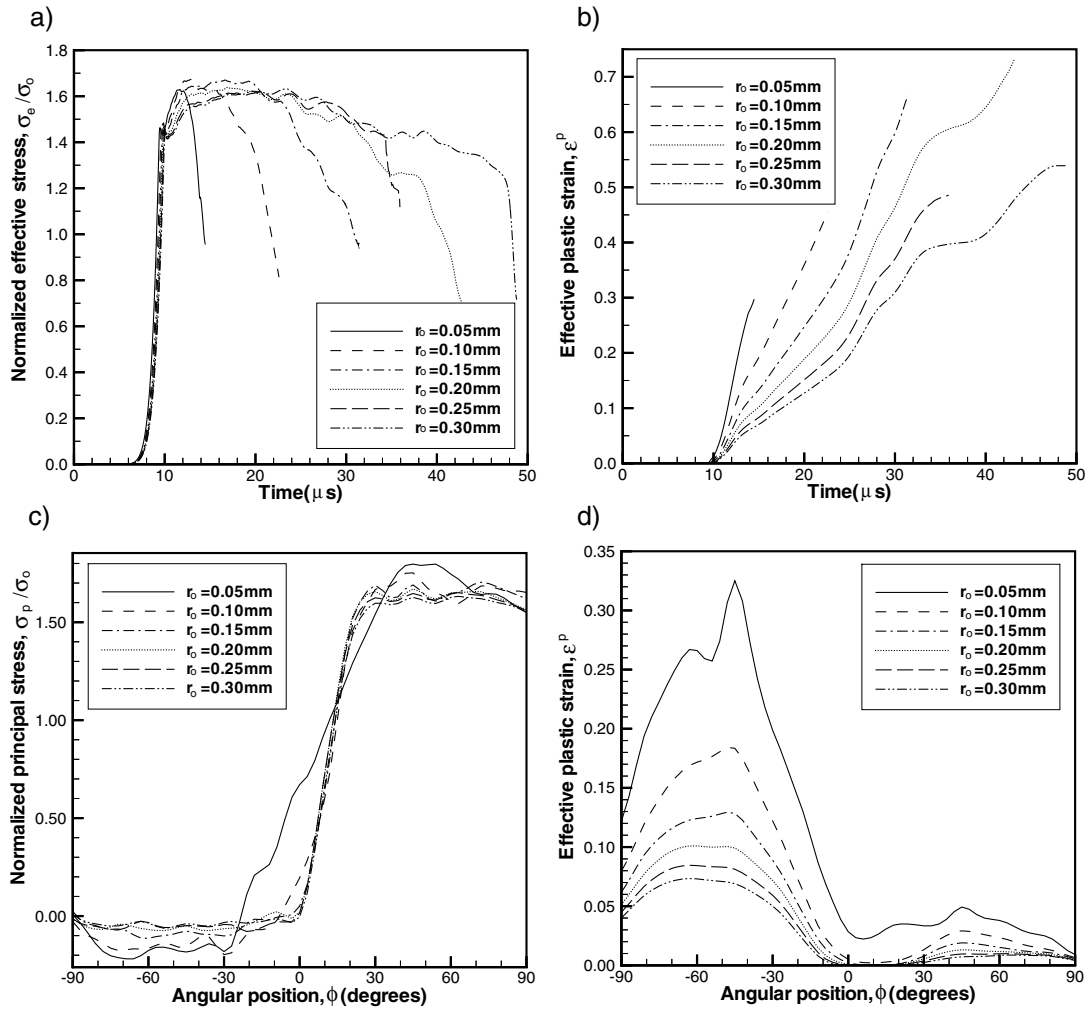


Figure 9. For the Bodner–Partom relation, $v_0 = 20 \text{ m s}^{-1}$, and for the six values of the notch tip radius, r_0 , time histories at the point P of (a) the normalized effective stress, (b) the effective plastic strain, (c) and (d) the angular variation of the normalized maximum principal stress and the effective plastic strain at $t = 15 \mu\text{s}$.

and Gummalla (2000) found from their computed data that $\beta = -0.31$ and -0.43 at $t = 9$ and $9.5 \mu\text{s}$ respectively. Batra and Gummalla used a significantly finer mesh consisting of 4-node/rectangular elements than that employed herein; thus their values of ϵ^p were determined at a point closer to the surface of the notch tip than those found herein. The fringe plots of the effective plastic strain at $t = 25 \mu\text{s}$ in the region around the notch tip for different values of r_0 are qualitatively similar to each other and are omitted. They reveal that for each value of the notch tip radius, two shear bands emanate from a point on the notch surface – one band is essentially along the axis of the notch and the other is inclined at about 135° clockwise from the notch axis. Figures 9c and 9d exhibit at $t = 15 \mu\text{s}$ the angular variation of the normalized principal stress and the effective plastic strain for the six values of r_0 . It is evident that in each case the angular width of the intensely deformed region is approximately the same. Whereas for $r_0 = 0.05 \text{ mm}$, a shear band initiates at $t = 12.5 \mu\text{s}$, the time of initiation of a shear band is greater than $15 \mu\text{s}$ for the other values of r_0 . The value of the maximum principal tensile

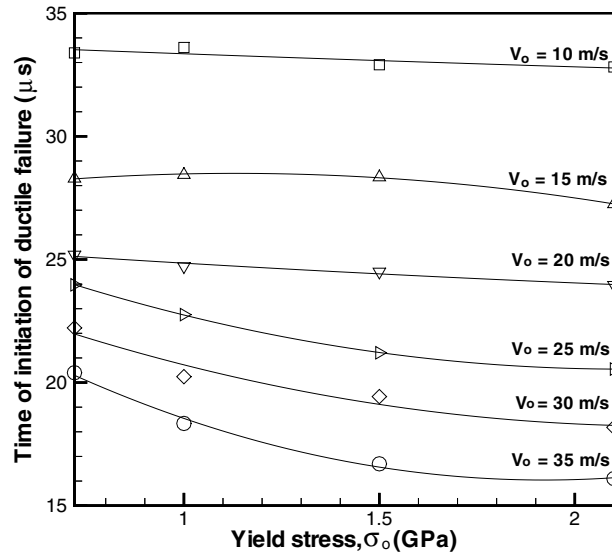


Figure 10. For the power law relation, the dependence of the time of initiation of the ductile failure upon the quasistatic yield stress of the material.

stress at $t = 15 \mu s$ is about the same for all values of r_0 . Note that the maximum value of the tensile principal stress occurs at a point slightly away from the notch tip surface.

8. Effect of the material strength

Shear stress vs. shear strain curves for simple shearing deformations of a homogeneous block plotted in Figure 3 of Batra and Gummalla's (2000) paper clearly indicate that as the quasistatic yield stress, σ_0 , of a steel increases the peak in the shear stress occurs at a lower value of the shear strain. This is because in a steel with a higher value of σ_0 more heat is produced for the same value of the effective plastic strain, and the material softens quicker. It suggests that a shear band will form at a lower value of the effective plastic strain as the quasistatic yield stress of the material is increased. This is confirmed by the plot of the time of initiation of a shear band or the ductile failure vs. σ_0 exhibited in Figure 10 for different values of the impact speed; these results are computed with the power law. The reason for switching from the Bonder–Partom relation to the power law is that in the Bodner–Partom relation the dependence of K_1 and K_0 upon σ_0 is not known. We note that for impact speeds in the range of 10 to 20 $m s^{-1}$, the time of initiation of a shear band is essentially unaffected by the value of σ_0 , but for a higher impact speed, the time of initiation of a shear band decreases noticeably as σ_0 increases. However, the time of initiation of the brittle failure increases with an increase in the value of σ_0 , but the relationship between the two is not monotonic. A similar trend was computed by Batra and Gummalla (2000) with the Johnson–Cook relation. Figures 11a and 11b depict for $v_0 = 20 m s^{-1}$ and for different values of σ_0 , the time histories of the evolution of the normalized effective stress and the effective plastic strain at the point P . It is evident from these plots that the initial effective plastic strain rate at the point P decreases with an increase in the value of σ_0 ; results for the material with $\sigma_0 = 0.3 GPa$ do not follow the pattern of results for other values of σ_0 . Batra and Gummalla (2000) noticed this too. We have plotted in Figures 11c and 11d the angular variation of the normalized principal stress

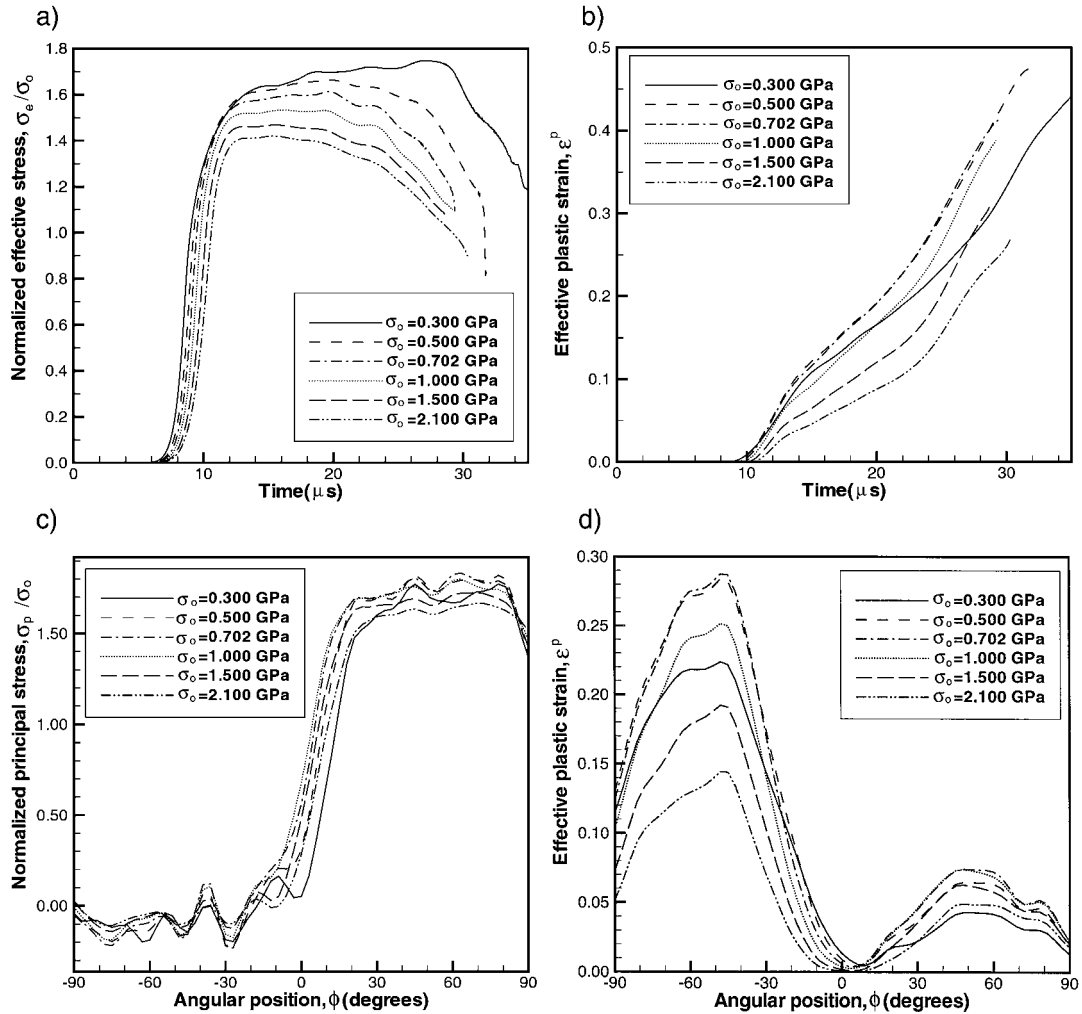


Figure 11. For $v_0 = 20 \text{ m s}^{-1}$, $r_0 = 0.15 \text{ mm}$ and different values of σ_0 , the time histories of the evolution of (a) the normalized effective stress, and (b) the effective plastic strain at the point P ; at $t = 25 \mu\text{s}$, angular variation of (c) the normalized principal stress, and (d) the effective plastic strain at points abutting the surface of the notch tip.

and the effective plastic strain at $t = 25 \mu\text{s}$ computed at the centroids of the elements abutting the surface of the notch tip. Whereas the peak values of the normalized principal stress vary between 1.6 and 1.8, those of the maximum effective plastic strain decrease from 0.29 to 0.14 as σ_0 is increased from 0.5 to 2.1 GPa. The angular position of the point where these peak values occur is essentially unaffected by the value of σ_0 .

9. Conclusions

We have used four thermoviscoplastic relations to analyze the thermomechanical deformations of a pre-notched plate impacted on the notched side by a cylindrical projectile. The action of the projectile on the plate is simulated by prescribing on the contact surface null tangential tractions and the time history of the normal component of the velocity. The thermoviscoplastic

relations are calibrated to give the same stress-strain curve during homogeneous simple shearing deformations of a block deformed at a nominal strain-rate of 3300 s^{-1} . The deformations of the pre-notched plate are nonhomogeneous and the time-dependent effective plastic strain rates at points near the notch tip attain values in the range of 10^4 s^{-1} . Results computed near the notch tip with the four thermoviscoplastic relations agree qualitatively but the magnitudes of the maximum effective plastic strain, the maximum principal tensile stress, the times when the effective stress at a point has dropped to 90% of its peak value there, and the time of initiation of the brittle failure as signified by the maximum principal tensile stress attaining a prespecified critical value are different. In a pre-notched plate made of a mild steel with a notch tip radius of 0.15 mm, the impact speed at which the failure mode transitions from brittle to ductile is found to be 13.5, 18.5, 19.3 and 22.9 m s^{-1} , respectively, for the Litonski–Batra, the power law, the Bodner–Partom and the Johnson–Cook relations. We should add that these values depend upon the criteria assumed for the initiation of the brittle and the ductile failure modes. For the Bodner–Partom relation, the transition speed is given by $1179 r_0^{0.465} \text{ m s}^{-1}$ when r_0 is in meters. From his test data on plates made of a high strength steel, Kalthoff found the transition speed to be $1350\sqrt{F_0} \text{ m/s}$ which equals 16.53 m s^{-1} for $r_0 = 0.15 \text{ mm}$. For a fixed value of the impact speed, the time of initiation of a shear band decreases with an increase in the value of the quasistatic yield stress of the material, and a decrease in the radius of the notch tip.

Acknowledgements

This work was supported by the ONR grant N00014-98-0300 to Virginia Polytechnic Institute and State University with Dr Y.D.S. Rajapakse as the program manager.

References

- Batra, R.C. (1988). Steady state penetration of thermoviscoplastic targets. *Computational Mechanics* **3**, 1–12.
- Batra, R.C. (1998). Numerical solutions of initial-boundary-value problems with shear strain localization, in *Localization and Fracture Phenomenon in Inelastic Solids* (Edited by P. Perzyna), Springer-Verlag, Wien, New York, 301–389.
- Batra, R.C. and Kim, K.H. (1990). Effect of viscoplastic flow rules on the initiation and growth of shear bands at high strain rates. *Journal of the Mechanics and Physics of Solids* **38**, 859–874.
- Batra, R.C. and Adam, Aslam (1991). Effect of viscoplastic flow rules on steady state penetration of thermoviscoplastic targets. *International Journal of Engineering Science* **29**, 1315–1331.
- Batra, R.C. and Kim, C.H. (1992). Analysis of shear bands in twelve materials. *International Journal of Plasticity* **8**, 425–452.
- Batra, R.C. and Ko, K.I. (1992). An adaptive mesh refinement technique for the analysis of shear bands in plane strain compression of a thermoviscoplastic solid. *Computational Mechanics* **10**, 369–379.
- Batra, R.C. and Jayachandran, R. (1992). Effect of constitutive models on steady state axisymmetric deformations of thermoelastic-viscoplastic targets. *International Journal of Impact Engineering* **12**, 209–226.
- Batra, R.C. and Jin, X.S. (1994). Analysis of dynamic shear bands in porous thermally softening viscoplastic materials. *Archives of Mechanics* **46**, 13–36.
- Batra, R.C. and Nechitailo, N.V. (1997). Analysis of failure modes in impulsively loaded pre-notched plates. *International Journal of Plasticity* **13**, 291–308.
- Batra, R.C. and Rattazzi, D. (1997). Adiabatic shear banding in a thick-walled steel tube. *Computational Mechanics* **5**, 442–426.
- Batra, R.C., Rajapakse, Y.D.S. and Rosakis, A.J. (eds.) (2000) Failure mode transitions under dynamic loading. A special issue of the *International Journal of Fracture* **101**, 1–180.

- Batra, R.C. and Chen, L. (2001). Effect of viscoplastic relations on the instability strain, shear band initiation strain, the strain corresponding to the minimum shear band spacing, and the band width in a thermoviscoplastic material. *International Journal of Plasticity* (to appear).
- Batra, R.C. and Gummalla, R.R. (2000). Effect of material and geometric parameters on deformations near the notch tip of a dynamically loaded prenotched plate. *International Journal of Fracture* **101**, 99–140.
- Batra, R.C. and Ravisankar, M.V.S. (2000) Three-dimensional numerical simulation of the Kalthoff experiment. *International Journal of Fracture* **105**, 161–186.
- Bodner, S.R. and Partom, Y. (1975). Constitutive equations for elastic-viscoplastic strain-hardening materials. *Journal of Applied Mechanics* **56**, 527.
- Budiansky, B. (1970). Thermal and thermoelastic properties of isotropic composites. *Journal of Composite Materials* **4**, 286–295.
- Chen, L. and Batra, R.C. (1999). The asymptotic structure of a shear band in mode-II deformations. *International Journal of Engineering Science* **37**, 895–919.
- Chu, C.C. and Needleman, A. (1980). Void nucleation effects in biaxially stretched sheets. *Journal of Engineering Materials and Technology* **102**, 249–256.
- Gurson, A.L. (1977). Continuum theory of ductile rupture by void nucleation and growth. Part I Yield criteria and flow rules for porous ductile media. *Journal of Engineering Materials and Technology* **99**, 2–15.
- Fischer, J.R. (1980). Void nucleation in spheroidized steels during tensile deformation. Ph.D. Thesis, Brown University.
- Hartley, K.A., Duffy J. and Hawley, R.H. (1987). Measurement of the temperature profile during shear band formation in steels deforming at high strain rates. *Journal of the Mechanics and Physics of Solids* **35**, 283–301.
- Hendrickson, J.A., Wood, D.S. and Clark, D.C. (1958). The initiation of brittle fracture in mild steel. *Transactions of the American Society for Metals* **50**, 656–681.
- Johnson, G.R. and Cook, W.H. (1983). A constitutive model and data for metals subjected to large strains, high strain rates, and temperatures. *International Symposium on Ballistics*, The Hague, The Netherlands, 1–7.
- Kalthoff, J.F. (1987). Shadow optical analysis of dynamic shear fracture. *SPIE, Photomechanics and Speckle Metrology* **814**, 531–538.
- Kalthoff, J.F. and Winkler, S. (1987). Failure Mode Transition at High Rates of Shear Loading, In: *Impact Loading and Dynamic Behavior of Materials*, (Edited by Chiem, C.Y., Kunze, H.D. and Meyer, L.W.) Verlag, **1**, 185–195.
- Kalthoff, J.F. (2000). Modes of dynamic shear failure in solids. *International Journal of Fracture* **101**, 1–31.
- Klopp, R.W., Clifton, R.J. and Shawki, T.G. (1985). Pressure-shear impact and the dynamic viscoplastic response of metals. *Mechanics of Materials* **4**, 375–385.
- Kobayashi, H. and Dodd, B. (1989). A numerical analysis of the formation of adiabatic shear bands including void nucleation and growth. *International Journal of Impact Engineering* **8**, 1–13.
- Lee, Y.J. and Freund, L.B. (1990). Fracture initiation due to asymmetric impact loading of an edge cracked plate. *Journal of Applied Mechanics* **57**, 104–111.
- LeRoy, G.H. (1978). Large scale plastic deformation and fracture for multiaxial stress states. Ph.D. thesis, McMaster University.
- Litonski, J. (1977). Plastic flow of a tube under adiabatic torsion. *Bulletin de L'Academie Polonaise Des Sciences, serie des Sciences Techniques* **XXV**, 7.
- Marchand, A. and Duffy, J. (1988). An experimental study of the formation process of adiabatic shear bands in a structural steel. *Journal of the Mechanics and Physics of Solids* **36**, 251–283.
- Mason, J.J., Rosakis, A.J. and Ravichandran, G. (1994). Full field measurements of the dynamic deformation field around a growing adiabatic shear band at the tip of a dynamically loaded crack or a notch. *Journal of the Mechanics and Physics of Solids* **42**, 1679–1697.
- Needleman, A. and Tvergaard, V. (1995). Analysis of brittle-ductile transition under dynamic shear loading. *International Journal of Solids and Structures* **32**, 2571–2590.
- Passman, S.L. and Batra, R.C. (1984). A thermomechanical theory for a porous anisotropic elastic solid with inclusions. *Archives of Rational Mechanics and Analysis* **87**, 11–33.
- Perzyna, P. (1986). Constitutive modeling for brittle dynamic fracture in dissipative solids. *Archives of Mechanics* **38**, 725–738.
- Ravi-chandar, K., Lu, J., Yang, B. and Zhu, Z. (2000). Failure mode transitions in polymers under high strain rate loading. *International Journal of Fracture* **101**, 33–72.

- Ritchie, R.O., Knott, J.F. and Rice, J.R. (1973). On the relationship between critical tensile stress and fracture toughness in mild steel. *Journal of the Mechanics and Physics of Solids* **21**, 395–410.
- Tvergaard, V. and Needleman, A. (1984). Analysis of the cup-cone fracture in a round tensile bar. *Acta Metallurgica* **32**, 157–169.
- Tvergaard, V. (1981). Influence of voids on shear band instabilities under plane strain conditions. *International Journal of Fracture* **17**, 389–407.
- Tvergaard, V. and Needleman, A. (1986). Effect of material rate sensitivity on failure modes in the Charpy V-notch test. *Journal of the Mechanics and Physics of Solids* **34**, 213–241.
- Tvergaard, V. and Needleman, A. (1993). An analysis of the brittle-ductile transition in dynamic crack growth. *International Journal of Fracture* **59**, 53–67.
- Zhou, M., Rosakis, A.J. and Ravichandran, G. (1996a). Dynamically propagating shear bands in prenotched plates: I – experimental investigations of temperature signatures and propagation speed. *Journal of the Mechanics and Physics of Solids* **44**, 981–1006.
- Zhou, M., Ravichandran, G. and Rosakis, A.J. (1996b). Dynamically propagating shear bands in prenotched plates: II – finite element simulations. *Journal of the Mechanics and Physics of Solids* **44**, 1007–1032.